MIDAS

MANAGING IMPACTS OF DEEP SEA RESOURCE EXPLOITATION

Project acronym:	MIDAS
Grant Agreement:	603418
Deliverable number:	Deliverable 2.2
Deliverable title:	Near-field hydrodynamic modelling of two case study sites
Work Package:	WP2
Date of completion:	20 April 2015

MIDAS MANAGING IMPACTS OF DEEP SEA RESOURCE EXPLOITATION

Near-field hydrodynamic modelling of two case study sites

Deliverable 2.2

D. Aleynik, A.C. Dale, M.E. Inall

Scottish Association for Marine Science,
Scottish Marine Institute,
Oban, Argyll,
PA37 1QA,
UK.

30 April 2015

Contents

1. Introduction

Deep ocean bottom boundary flows are often highly complex, dynamic and turbulent [*Dale and Inall, 2015*]. On the abyssal plains, bottom flows reflect large-scale ocean circulation, as well as tides, transient eddies, fronts, and near-inertial waves originating at the ocean surface. In topographically-complex regions, mixing-driven residual flows also become important. Stratification is typically weak (low value of the buoyancy frequency, N) which means that even the relatively slow flows of the deep ocean (a few cm s^{-1}) can create turbulent disturbances which originate from the bottom boundary and may penetrate a hundred metres or more vertically.

There is some potential for generically characterising deep ocean sites in terms of their hydrodynamic regimes [see Deliverable 2.1: Categorisation of deep sea sites according to the effect of local hydrodynamics on the near-field dilution of mining discharges]. However, the complexity of near bed flows means that for detailed predictions of plume structure, behaviour and dispersion, local numerical modelling is required at very high resolution (of order 100 m), and in three dimensions.

In ocean circulation models, the hydrostatic approximation is frequently made for reasons of computational efficiency. This approximation breaks down when considering small flow structures in which timescales become comparable to the buoyancy timescale N^{-1} (typically of order hours in the deep ocean). For flow past a bathymetric feature, advection sets a timescale L/U (where L is a lengthscale for the topography and U is a velocity scale). For deep ocean flow speeds ($U \sim 0.05$ ms^{-1}) features of hundreds of metres or less in extent produce non-hydrostatic flow responses. Other phenomena with small-scale structure, such as internal waves and tides interacting with slopes also display non-hydrostatic dynamics. The deep ocean is rich in structure on these scales, and, for this reason, a non-hydrostatic modelling approach is essential when considering plume behaviour on these scales. The MITgcm [*Marshall et al., 1997*] is the most developed finite-volume, non-hydrostatic ocean modelling tool and is ideally suited to modelling deep ocean boundary layer flow.

The high resolution hydrodynamic modelling reported here has been focused on the near-field dynamics of a passive plume around two contrasting target sites:

- The Rainbow vent field, at a depth of 2.5 km in a topographically complex region of the Mid Atlantic Ridge.
- A CCZ segment in the Pacific, centred near 11^0N, 116^0W, an abyssal region with a characteristic depth of about 4 km and scattered, isolated topographic features.

This report is structured as follows: Section 2 describes the model configuration, including initial and boundary conditions; Sections 3 and 4 present model simulations of: 1) a typical SMS deposit region on the MAR (mid-Atlantic Ridge), and 2) a polymetallic nodule region of the CCZ (Clarion Clipperton Fracture Zone). Further planned model simulations and diagnostics, which will be produced as a later supplementary report, are discussed in Section 5.

2. MITgcm model configuration

The model rectangular domain has been centred at target sites with a grid of 192x192 cells in a box with sides 45 x 45 km for both sites. Horizontal resolution is 200 m in the majority (85%) of the model domain. However, a telescopic increase in horizontal grid spacing was introduced, up to 1 km at the lateral open boundary (Figure 3), aiming to reduce the influence of spurious reflection of internal waves back into the model domain. This grid stretching was performed using a shifted hyperbolic tangent function [*Dunphy, 2009*]. To cope with horizontal pressure gradient errors [*Haney, 1991*] a finite-volume 'partially-shaved cell' treatment (discretization) of irregular topography, a rival of vertical sigma-coordinate systems, was applied, with a coefficient F_{Min}=0.2 for cells intersecting the topography. The model of the Rainbow site has 80 vertical layers with enhanced vertical resolution (20 m) in the upper 100m, and between 1.5 and 2.5 km, and 100 m elsewhere. For the Pacific site (CCZ), the model has 90 vertical layers with enhanced vertical resolution (20 m) in the upper 100m and below 3.4 km, and 100 m elsewhere.

The model simulations were initialised with potential temperature and salinity derived from smoothed CTD profiles. For the equation of state we selected the modified [*Jackett and McDougall, 1995*] formula of buoyancy $b(\theta,S,r) = \frac{g}{\rho_c}(\rho_c(\theta,S,r) - \rho_c)$, where θ is the potential temperature, ρ_c is reference density, g is gravitational acceleration and r is the vertical coordinate.

Locally generated nonlinear internal waves can lead to strong velocity shear and mixing. The "PP" scheme [*Pacanowski and Philander, 1981*], with a Richardson-number (*Ri*) dependant parameterisation for turbulent closure, is an appropriate parameterisation of vertical viscosity ϑ and diffusivity k:

$$\vartheta = \frac{\vartheta_0}{(1+\alpha Ri)^n} + \vartheta_b;\ k = \frac{\vartheta}{(1+\alpha Ri)} + k_b \qquad (1)$$

where $Ri = \frac{N^2}{\left(\frac{\partial u}{\partial z}\right)^2 + \left(\frac{\partial v}{\partial z}\right)^2}$, and $N^2 = -\frac{g}{\rho}\left(\frac{\partial \rho}{\partial z}\right)$ is buoyancy frequency, v_b=10^{-5}m^{2}s^{-1} and k_b=10^{-5} m^{2}s^{-1} are background values and constants v_o=1.5·10^{-5}m^{2}s^{-1}, α=5, n=1.

Horizontal eddy viscosity and diffusion coefficients were set to K_h=0.1 m^{2}s^{-1}. This estimate is comparable to the values used for similar small-scale horizontal grids [*Stashchuk et al., 2014*]. For short time steps, with low values of the Courant (CFL) number $c=u\cdot\Delta t/\Delta x \approx 0.0015$, second order non-linear flux limiter advection schemes, such as 'Superbee' [*Roe, 1985*], are preferable [*Marshall et al., 1997*] and we applied this for most plume-release experiments. However, we also performed test runs with higher accuracy, third order direct space-time (DST) advection methods, with and without the non-linear limiters, for tracer released from two sites at the CCZ and found that performance with limiters is very close to the 2nd order non-linear flux limiter advection scheme results. An example of tracer advection schemes tested in the CCZ domain is given in Figure 1.

To simulate the tidal velocities measured by ADCP current meters, we added an extra term to the model momentum balance equations - the tidal potential values - which we computed with 8 major tidal constituents (M_2, S_2, N_2, K_2, K_1, O_1, P_1, Q_1) using the TPXO7.2 global dataset and OSU inverse tidal model [*Egbert and Erofeeva*, 2002] for the mooring location. The duration of simulations was restricted to several weeks at both model sites. Models start from a state of rest and implement a short ramping period (1-3 hours) to eliminate spurious currents.

Model integration time requires 48 hours of wall time to perform 5 days of simulation and produces 0.3Tb output at the Cray XC30 ARCHER system using 384 cpus (16 nodes of Intel 2.7 GHz, 2x12-core E5-2697 v2 (Ivy Bridge) 64Gb RAM).

Table 1: *MITgcm configuration summary for modeling sites near the Rainbow vent field on the Mid Atlantic Ridge (MAR) and in the Clarion-Clipperton fracture Zone (CCZ) in the northern tropical Pacific.*

Model parameters	**units**		**MAR**	**CCZ**
Grid		X×Y×Z	192x192x80	192x192x90
Resolution at target area	m	X×Y×Z	200x200x20	200x200x20
Background horizontal viscosity	$m^2 \cdot s^{-1}$	A_h	0.0, 0.5, 100	0.1
Background horizontal diffusivity	$m^2 \cdot s^{-1}$	K_h	0.0, 0.5, 100	0.1
Vertical mixing scheme for sub-grid viscosity and diffusivity		Ar Kr	[*Pacanowski & Philander, 1981*]	
Tracer advection scheme			77[1]	77[1],33[2]
MITgcm packages used:		pp81,	obcs, rbcs,	ptracer, exf
Background velocity	m/s		NE fixed flow, 0.05	daily averaged ADCP, 0.03-0.12
Tidal forcing , 8 constituents			TPXO	TPXO
Time steps	seconds		6.0	6.0
Output frequency	seconds		600; 3600	600; 3600
Tracer source			constant	discreet

[1] *The second order Flux Limiters non-linear 'Superbee' [Roe, 1985].*
[2] *The third order direct space-time (DST) with flux limiter non-linear.*

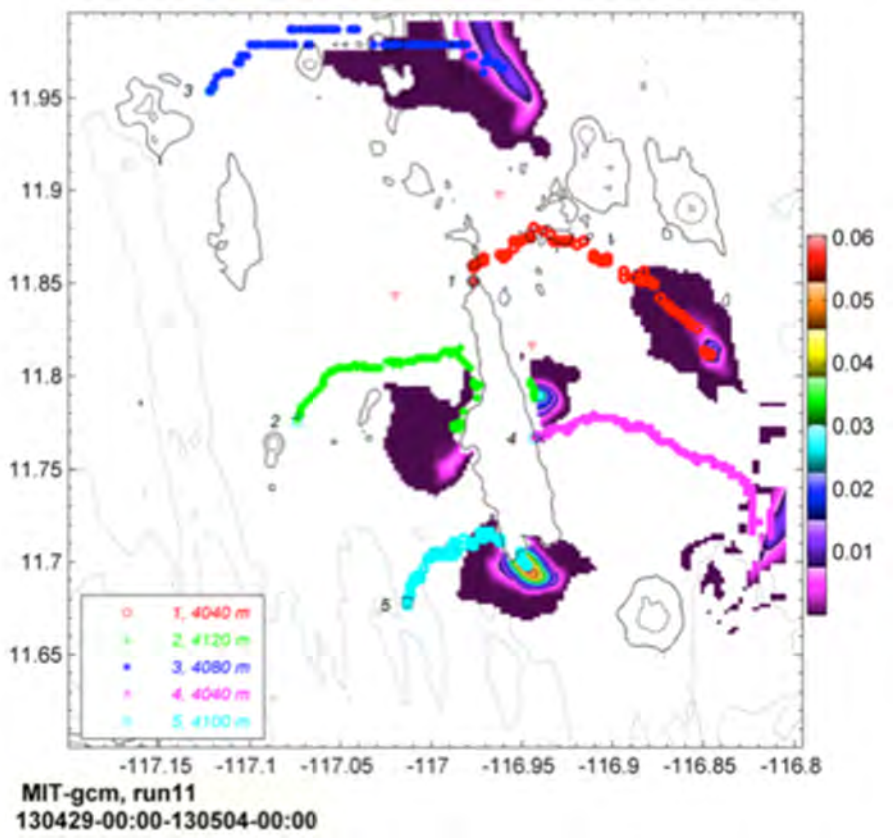

Figure 1: Plume centre of mass movement during period II (see Figure 11), using differing tracer advection schemes. A 'burst' mode is used, with sources located at the centre of the mooring triangle (1), at two mixing 'hot spots' (2,3) and elsewhere (4,5). The final plume distribution is shown by filled contours. Black contours show bathymetry. Tracer advection schemes used were:

(1, 2, 3): 2nd order Flux Limiter, non-linear [Roe,1985];
(4): 3rd order DST Flux Limiter, linear;
(5): 3rd order DST Flux Limiter non-linear.

3. MAR Simulations

The MITgcm model setup for the Rainbow region of the MAR (Figure 2) comprises a domain centred at a vent field site (36^0 14' N 33^0 54' W) and located within a narrow (few km wide) rift valley with steep side walls rising to 1-2 km above the central segment. The model design allows it to run both on ARCHER (UK national super computer resource) and on a local in-house HPC cluster at SAMS. The model grid is stretched telescopically in the horizontal plane (Figure 3) and topography is interpolated from a 50x50 m grid based on Global Multi-Resolution Topography available at MGDS [http://www.marine-geo.org/tools/maps_grids.php] (Figure 4). To fill the model basin with initial potential temperature and salinity we used smoothed profiles (Figure 5a) from a deep CTD station obtained within the MAR rift valley ~4 miles south-west of the Rainbow vent site on 14th May 2014 during Pelagia PE388 cruise and kindly provided by NIOZ (courtesy A. Rabitti). Background velocity, estimated from a historical dataset [*Thurnherr, 2006; Thurnherr et al., 2002*], was added to simulate circulation within the rift valley, in addition to tidal forcing based on TPXO7.2. With recent recovery of the moorings deployed in May 2014, model runs will be updated using a daily-averaged flow for validation purposes.

Model results for the MAR site demonstrate that currents within the rift valley generally follow topography in a North-eastward direction. Tidal analysis was performed and M2 ellipses (Figure 6a) reveal variations associated with topography. A complicated pattern of near-bottom currents, with recirculating eddies and enhanced speed in narrows (such as north of the Rainbow central axial elevation) was also captured by the model. Flow field snapshots are shown on a horizontal map (Figure 7a) and along a vertical transect (Figure 7b) above the hydrothermal vent system.

Simulation of plume dispersal is based on constant pumping of the tracer form the source. In a vertical plane it spreads along isopycnal surfaces with weak vertical diffusion (Figure 7b). 2D and 3D tracer fields after 5 and 9 days from the beginning of the model run are shown in Figure 8. The model was capable of reproducing along-axis spreading in the NE direction, which matches well previous optical observations.

Non-linear Internal Waves (IW) are generated as a result of tidal interaction with the steep slopes of multiple topographic features within the rift valley and its walls (Figure 9a). The model was capable of reproducing two types of IW: a) *spiral* type generated at smaller-scale bumps and cavities; and (b) elongated *Quasi-planar* internal waves that are formed mostly generated at canyon walls. Both types of IW propagate with a speed 30-35 $cm \cdot s^{-1}$

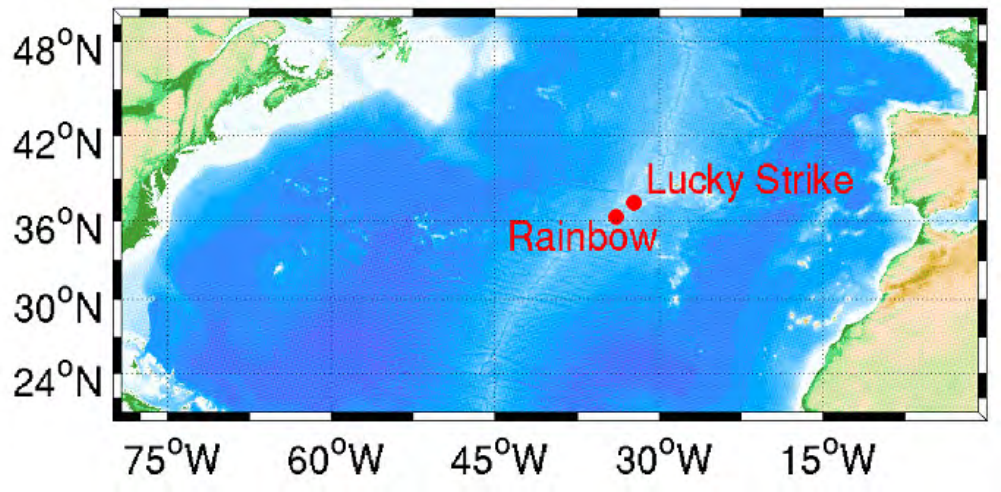

Figure 2: Bathymetric map of subtropical north Atlantic indicating Rainbow (modelled) and Lucky Strike (not modelled) regions.

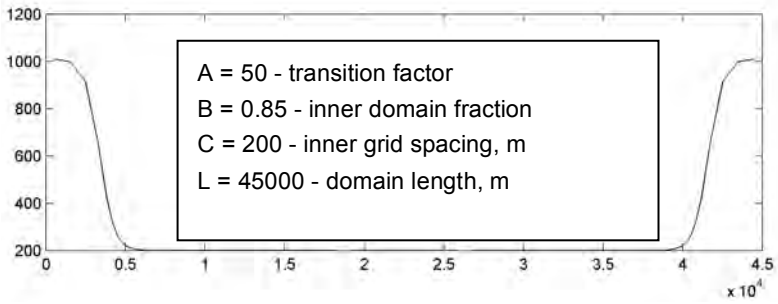

Figure 3: Horizontally stretching grid size (m) within the MITgcm model domains for the MAR and CCZ.

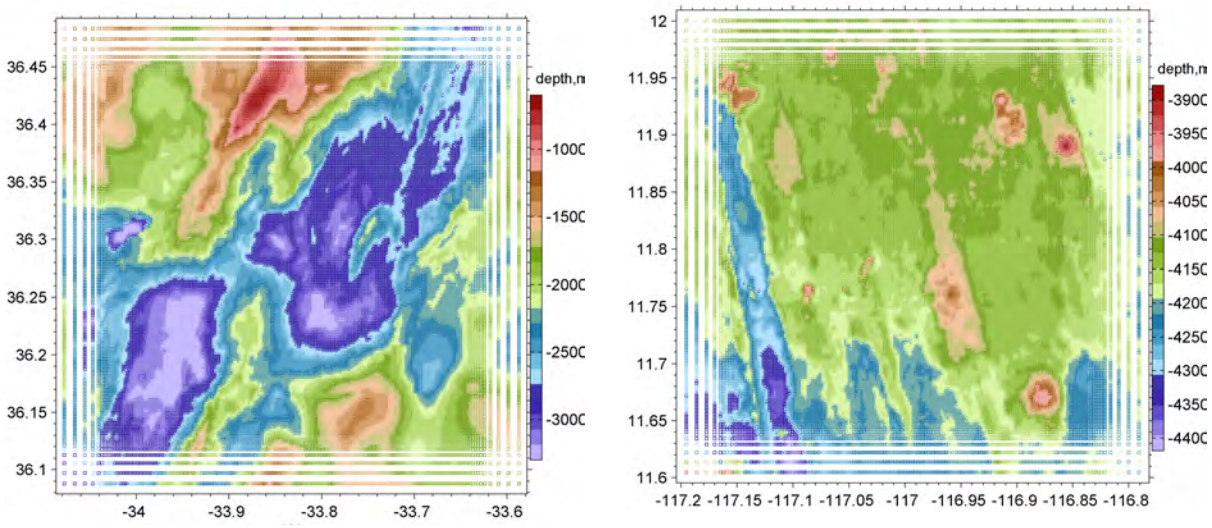

a *b*

Figure 4: MITgcm Rainbow (a) and CCZ (b) model domains bathymentry based on MGDS data (a) and Multibeam mapping survey performed with R/V Kilo Moana during MANAGAN 2008 campaign [Wiedicke-Hombach and al., 2009].

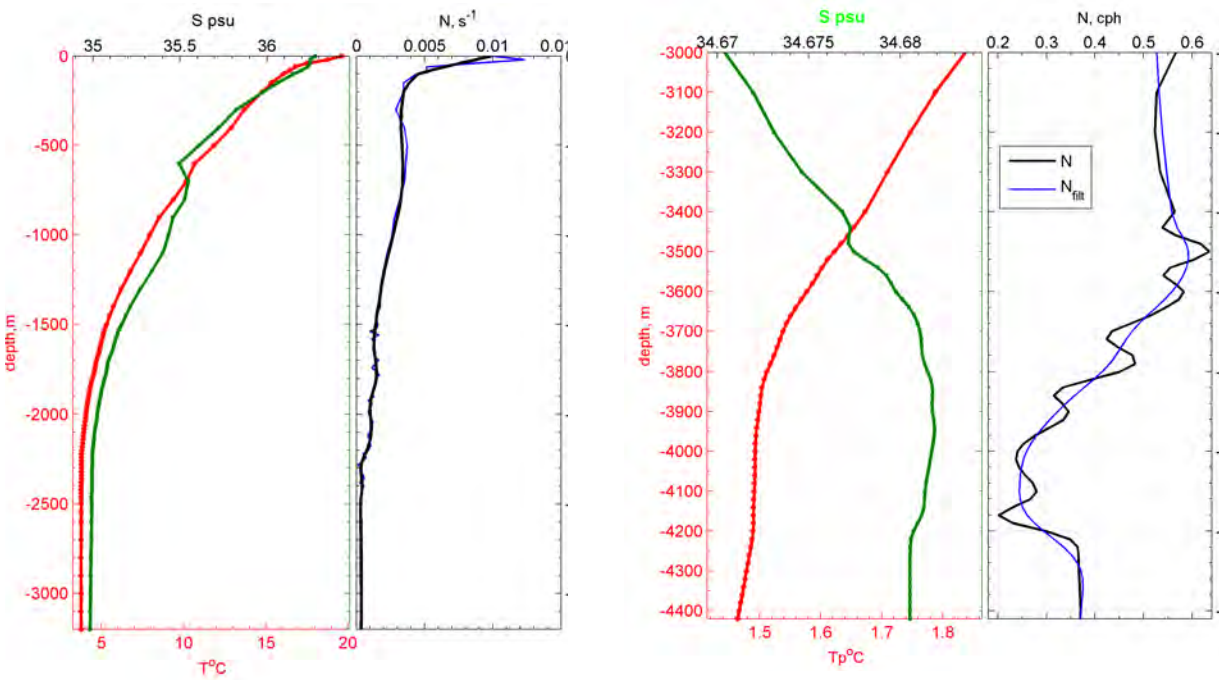

a b

Figure 5: Inital potential temperature θ (°C), salinity S and buoyancy frequency (N, s^{-1}) profiles within Rainbow rift valley model domain based on CTD station #11, May 2014, RV Pelagia (a). Deep segment of the potential (relative 4200 m) temperature θ_4, salinity S, and squared buoyancy frequency (N,cph) profiles at CTD station #55, 26.04.2013, MANGAN 2013, RV Kilo Moana (b), both re-interpolated at MAR and CCZ models vertical grid.

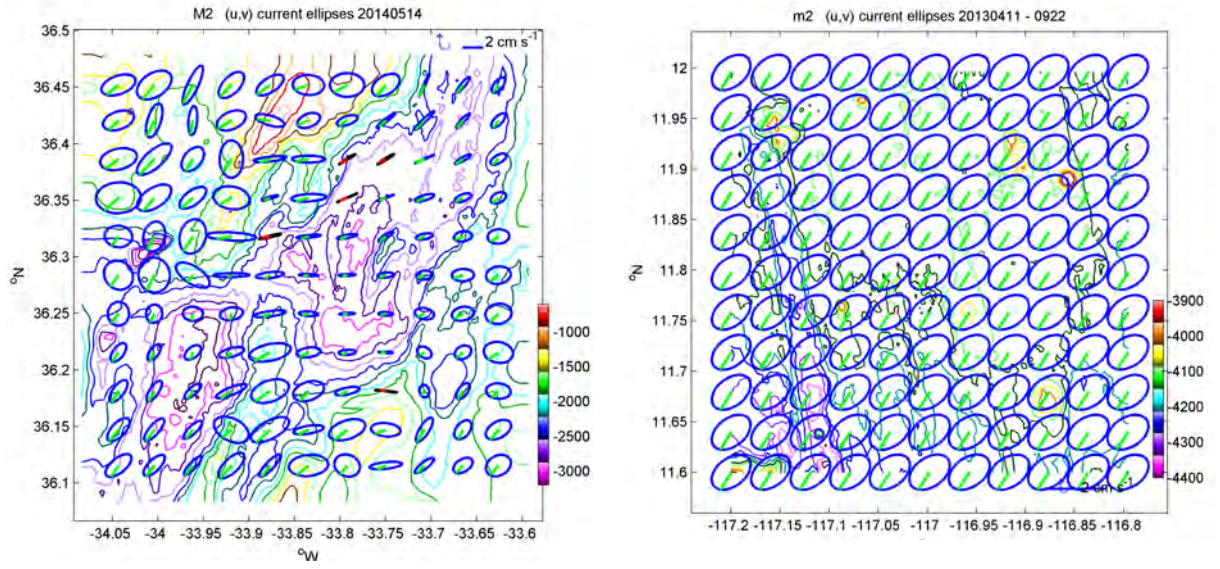

a b

Figure 6: Tidal ellipses (M_2) for (a) the MAR domain and (b) the CCZ domain.

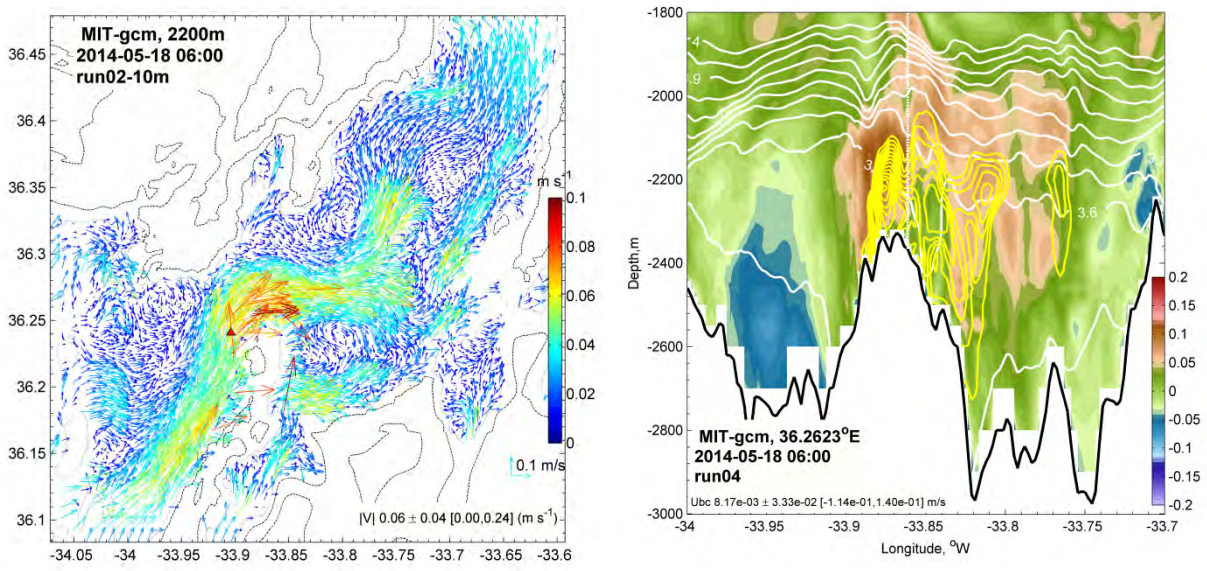

Figure 7: (a) Snapshot of the velocity field at 2200m depth within the rift valley of the MAR after 5 days of model run. (b) Vertical section of east/west baroclinic currents across the rift valley. The vertically-averaged component was subtracted from the full velocity profile. The colour scale is in m/s. Overlapping white lines shows vertical displacement of isotherms (°C), associated with Internal waves IW; yellow isolines indicate spread of a passive tracer emanating from 'black smokers'.

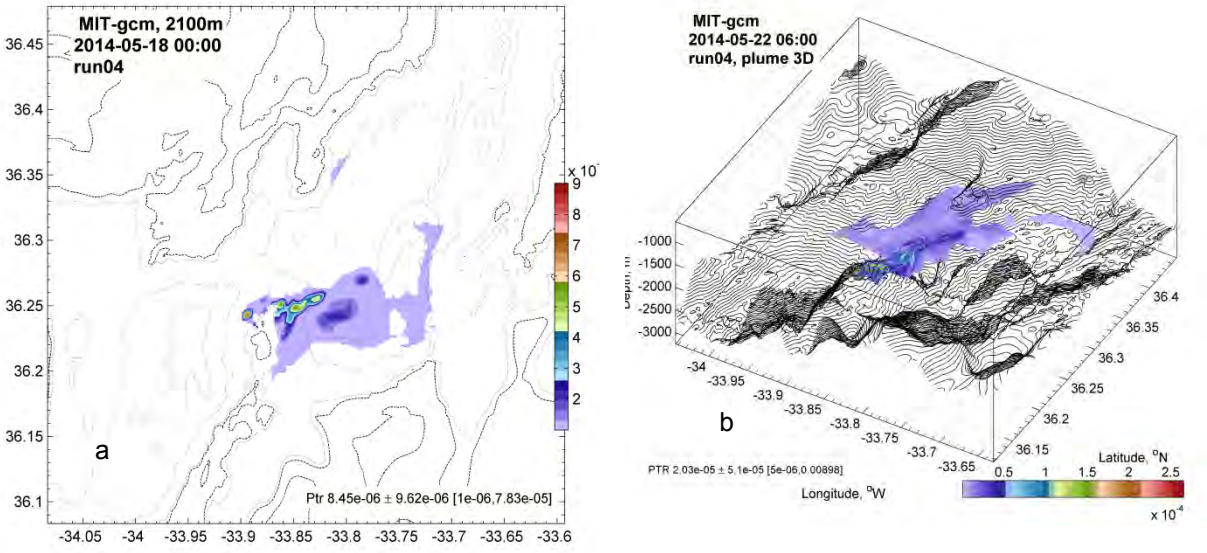

Figure 8: 2D and 3D snapshots of rising plume dispersal from the Rainbow hydrothermal vent field on the Mid Atlantic Ridge (36°14'N) after (a) 5 and (b) 9 days from the start of the simulation.

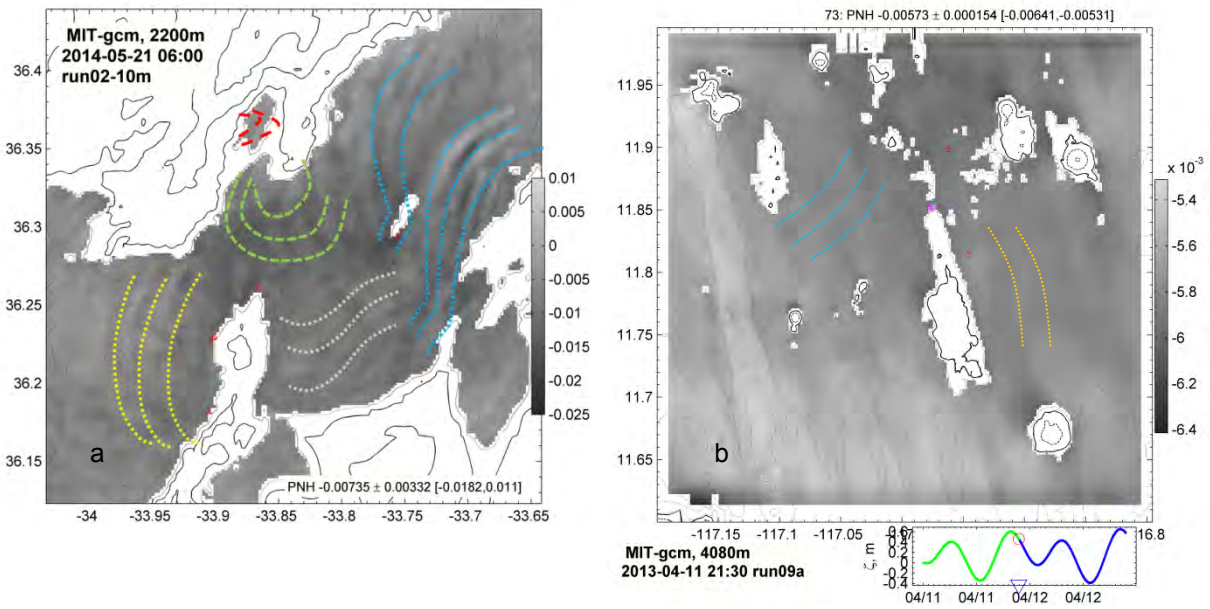

Figure 9: The horizontal distribution of the non-hydrostatic pressure (dbar) at a water depth of 2200m aids visualisation of upstream propagation of IWs, reflected from the topography of the MAR site (a) and much less pronounced at CCZ (b) where the bottom is flatter. ADCP moorings locations are indicated with a Δ. The MAR site reveal the presence of spiral type IWs (green, red) and Quasi-planar IWs (yellow and blue).

4. CCZ simulations

The CCZ (Figure 10) model setup comprises a rectangular domain of the same size as used for the MAR simulations (45x45 km) centred at the ADCP mooring location within a relatively flat abyssal plane with a 200-300 m deep trench parallel to its western boundary and several randomly distributed hills rising to a few hundred meters above surrounding abyssal areas (Figure 4b and Figure 10). Full depth CTD casts on the western periphery of the Eastern Pacific warm pool reflect the vertical structure and typical water mass distribution under the North Equatorial Current, which generally flows westward under the NE trade winds. The profiles of the deep lower part of potential temperature θ_4 relative to 4200 m, salinity *S*, and squared buoyancy frequency *N* (Figure 5b) were obtained at CTD station #55 (26.04.2013) two weeks after setting up the ADCP measurements. A thick quasi-homogeneous bottom boundary layer (BBL) extended more than 300 m above the sea-bed and occupied layers *z*=3800–4120 m with a range of values of θ_4 =1.465–1.483 ˚C and *S*=34.670 –34.682 psu. The main characteristics of stratification in deep water (below 3 km), including the fine structure, remain very similar during two days and 4 consecutive deep CTD casts (20–22 April 2014). The structure is, however, vertically displaced by 10-15 m by an internal tide. The mean temperature and salinity gradients in the weak pycnocline above the homogenous BBL layer (*z*=3400–3800 m) were T'=0.00035 ^{o}C·m^{-1}, S'=0.000015 psu·m^{-1} and the range of buoyancy frequency *N* varied between 0.24 and 0.6 cph (4.2-11.1×10^{-4} s^{-1}). Temperature sensors attached to three ADCP moorings demonstrate very stable values (1.39, 1.35 and 1.43 ^{o}C) with small variance σ±0.008 ^{o}C. The deepest original potential temperature and salinity profiles with 1 m vertical resolution have been re-interpolated onto the vertical grid (20 m near seabed) to produce initial hydro-physical model fields (Figure 5b).

On the 11th of April, 2013 a set of bottom-wired RDI-ADCPs (WH 600 kHz) was deployed at a depth of about 4120 m at the vertices of an equilateral (8 km) triangle centred at 11.86˚N, 116.97˚W, during the

MANGAN 2013 cruise [*Ruhlemann et al., 2014*]. Mooring locations are shown with red triangles on Figure 9b. The bathymetric map of the German license area for polymetallic nodule exploration was produced using a SIMRAD EM 120 swath mapping system mounted on R/V Kilo Moana [*Wiedicke-Hombach et al., 2009*] with 100 m resolution (Figure 4b). During 13 months, vertical profiles of zonal (u), meridional (v) and vertical (w) velocities with a 1-hour sampling rate and 1 m vertical resolution were collected at a depth range of ζ = 10-17 meters above the sea-bed (mab). The pitch and roll signals were very small (less than 1.5 degree), as well as their trends, therefore any special correction to horizontal velocity components was not applied. The vertical variability of temperature, salinity, oxygen, and fluorescence in the near sea-bed waters was obtained with eight CTD casts around the mooring sites using an SBE 911 plus instrument during 20-27th April 2013. This dataset was used to prepare the initial state of the CCZ model. Daily-averaged de-tided residual flow (Figure 11) was added at the model open boundaries in addition to tidal forcing, which was extracted for the CCZ model domain using TPXO7.2 and OSU model [*Egbert and Erofeeva, 2002*]. Model tidal ellipses are much more homogenous at the CCZ than at the MAR rift valley site (Figure 6b).

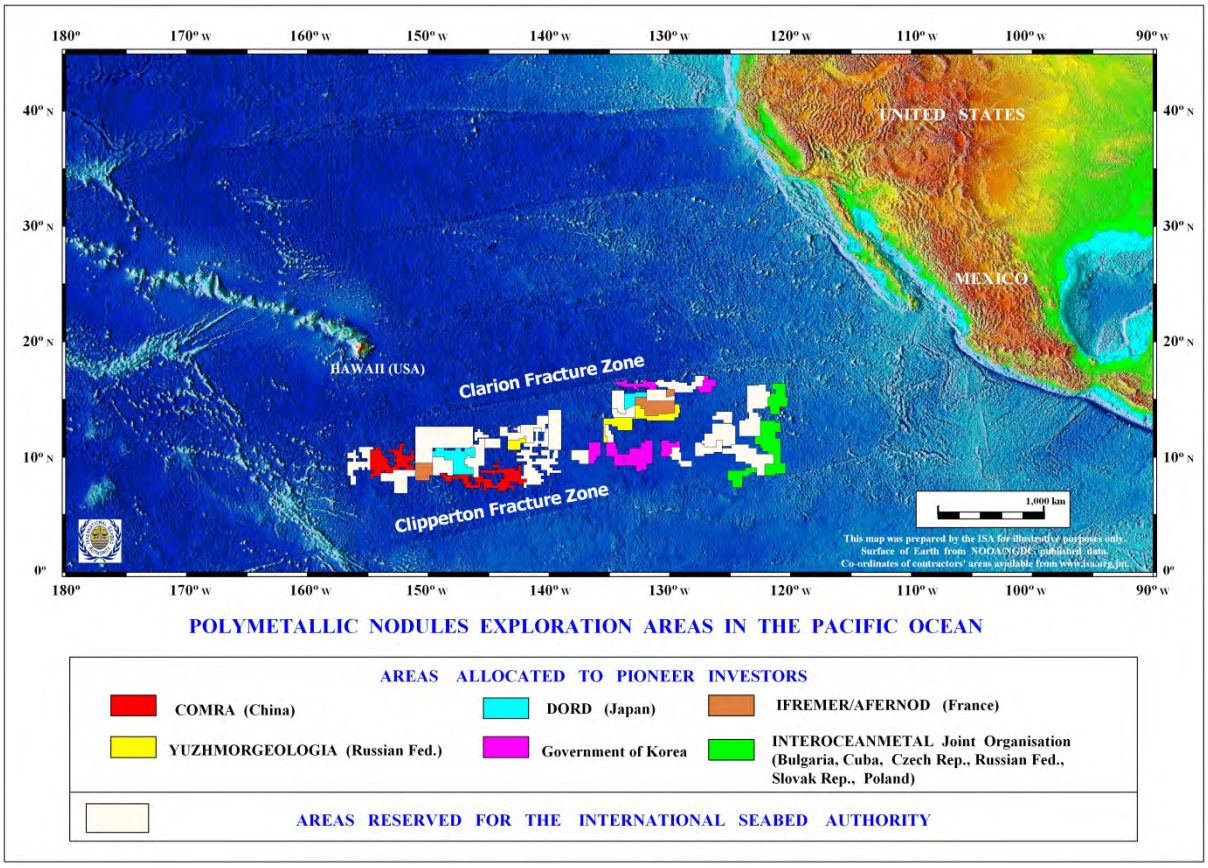

Figure 10: Bathymetric map of polymetallic nodule exploration areas in the Pacific ocean. Approximate location of the modelled area in the German zone is indicated with a star. Copyright ISA

Table 2. *MITgcm model runs for MAR and CCZ domains performed.*

#	Model experiments	MAR	CCZ
1	No tidal forcing	v	v
2	Tide only	v	v
3	Tide + residual flow historical	v	-
4	Tide + residual flow recently observed	-	v
5	Tide + residual flow + inertial	-	-
6	Tracer release permanently	v	v
7	Tracer release during 2 hours I period	-	v
8	Tracer release during 2 hours II period	-	v

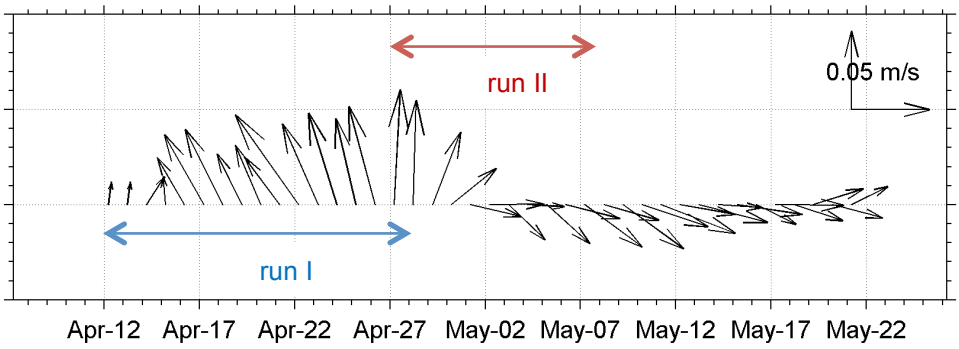

Figure 11: Extract of residual (daily-averaged) near-bottom currents from a 600kHz ADCP data in a layer 10-17 metres above bottom, for the period of the MITgcm model runs of the CCZ domain. April-May 2013. (Courtesy of BGR, A.Vink). This velocity record was used to force the model at its open boundaries for two periods: (I) during eddy propagation and (II) afterward.

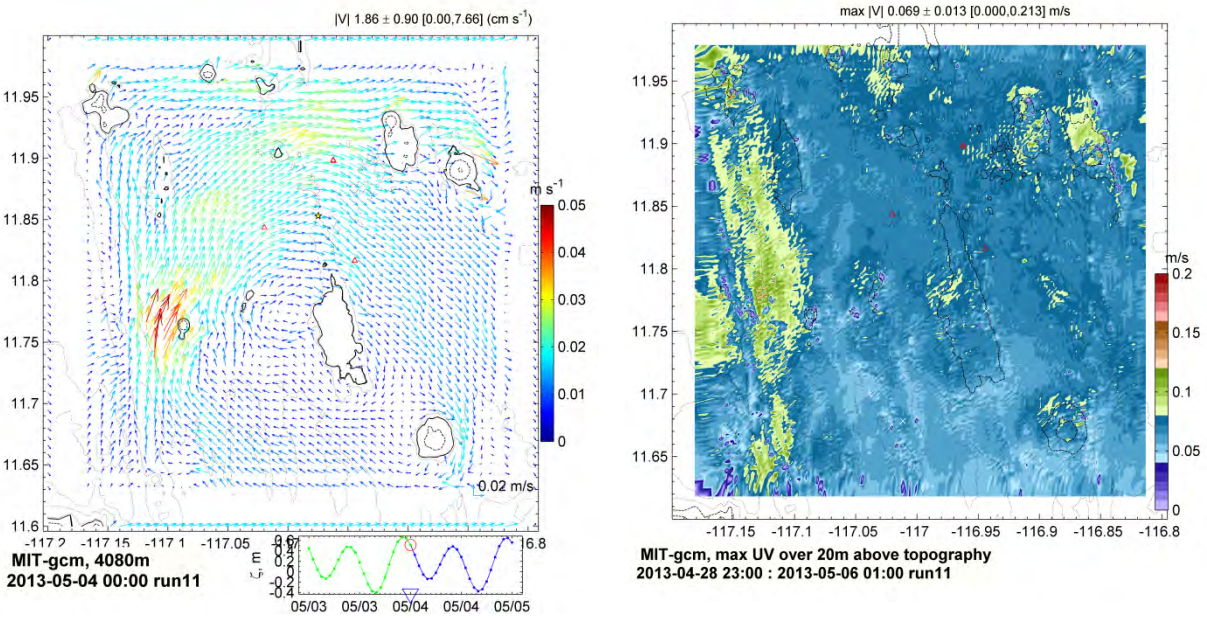

Figure 12: (a) Snapshot of the velocity field at 4080m depth within CCZ domain after 6 days of model run. (b) Peak flow distribution in a near-bottom layer extracted from 8 days model run.

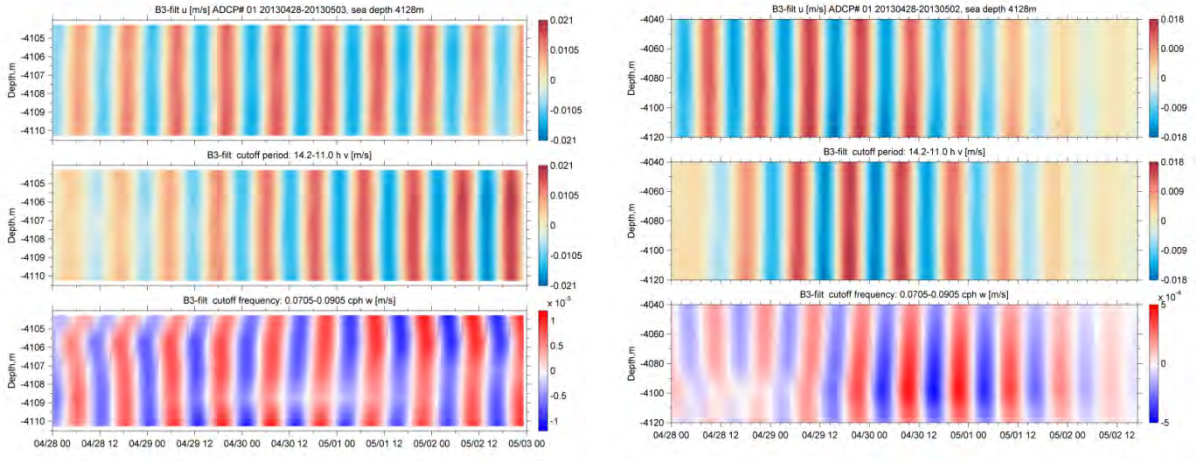

Figure 13: (a) Low-pass filtered zonal (u), meridional (v) and vertical (w) currents speed (m/s) during 5 days in spring 2013. A 6th-order Butterworth filter with cut-off frequency range f_o = 0.0705-0.0905 cph (cut-off period T_o = 14.2÷11.0 hours), in the semidiurnal M_2 range, was applied. (b)As (a) according to the MITgcm simulation. Note the depth range is higher.

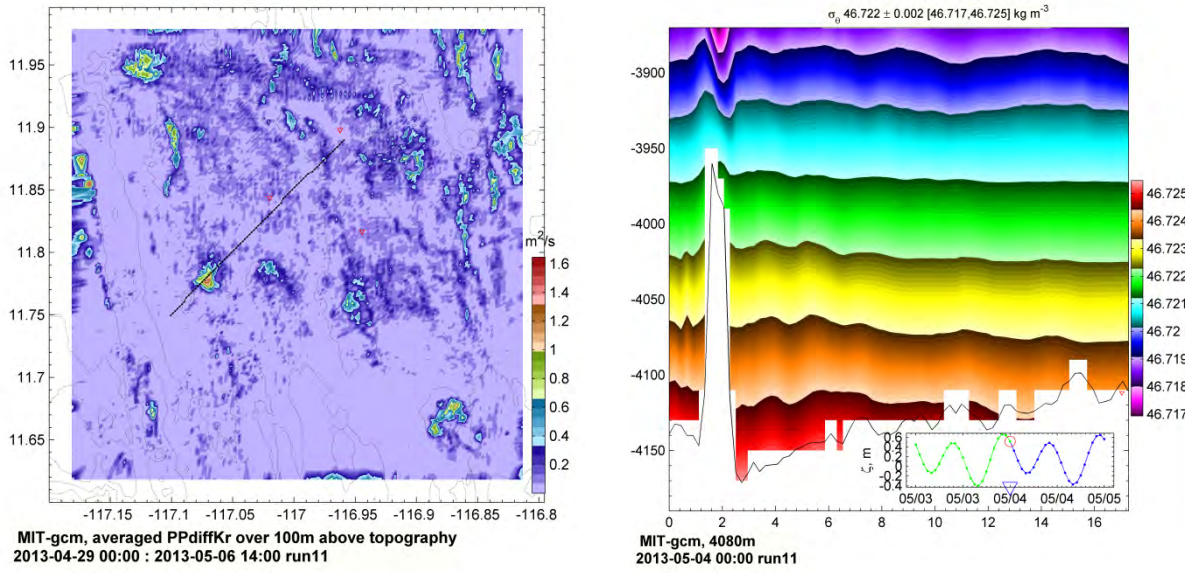

Figure 14: (a) MITgcm model: averaged vertical diffusion (PPdiffKr ×10^3 $m^2 \cdot s^{-1}$) in a layer 100 m above sea-bed over period II with dominant eastward mean flow (after the energetic eddy propagation). (b) Vertical potential density transect along the black line across one of the 'mixing hotspot'. Vertical displacement of isopycnal indicates the presence of Lee-waves behind the topographic bump.

Model results from the CCZ site demonstrate that tidal ellipses are unaffected by the presence of numerous small topographic bumps (Figure 6b), and that tidally generated internal waves are relatively weak compared with the CCZ (Figures 9 a and b). Analyses of current meter data from the near bed in the CCZ, undertaken to ensure correct model forcing, has revealed that oscillating flow at near-inertial frequency (centred on a period of 38.5 hours) are as energetic as tidal flows (Figure 15). The origin of oscillations a near-inertial frequencies is almost certainly the wind at the surface, and most likely non-locally generated, since the energy travel from the surface at a very small angle to the horizontal (a few degrees at most). This result was unexpected.

Although tidal patterns are largely unaffected by the topography, locally, the interaction between near bed flows (a combination of tidal, near-inertial and mean) and the topography is very pronounced in their vicinity (Figures 12 and 14). Weak near-bed flow patterns vary drastically on similar spatial scale to the topography, indicative of oscillatory (tide and/or near intertial) and/or mean flow interaction with topographic features (Figure 12a and b). The vertical expression of flow topography interaction, indicates that hydraulic lee waves may form downstream of a bump (Figure 14b), resulting in enhanced vertical mixing (or boundary layer thickness) downstream of even small topographic features (~100m high by a few km wide, see Figure 14a).

A further unexpected result was the effect of full depth ocean eddies on the mean (or slowly varying) near bed flow, and these are described in more detail now through a case study of one particularly intense eddy.

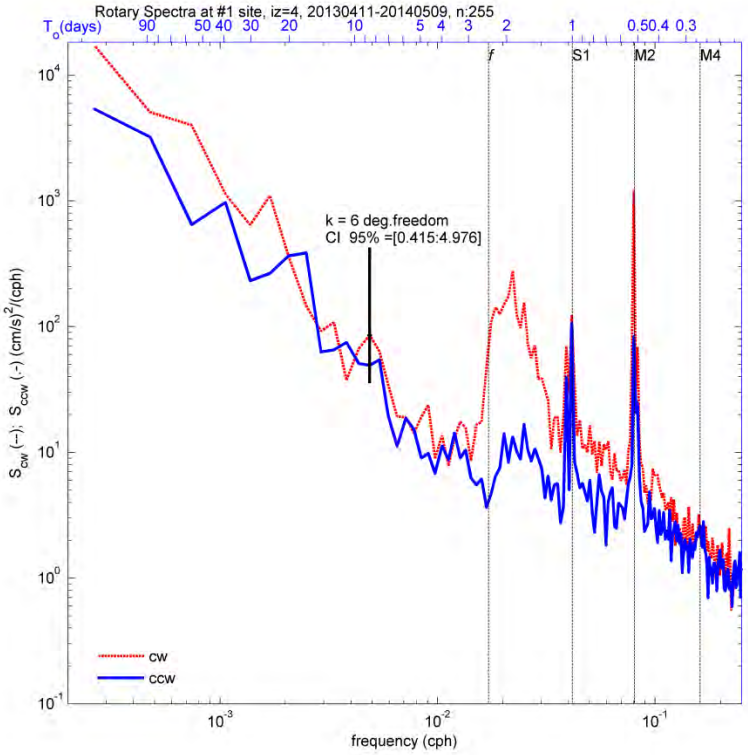

Figure 15: Rotary spectra of near-bed velocity components from mooring site #1 at the CCZ for the period 2013/04/11 to 2014/05/09. Clockwise (anticyclonic) motion is more energetic at almost all frequencies. High energy densities are found at M_2 and S_1 frequencies, and at f=0.026 cph (38.5h), which higher than the local inertial frequency f_i=0.0171 cph (58.4 h).

CCZ model case study: variations in modelled plume behavior resulting from a passing eddy

The Tehuantepecer is a cool, dry northeasterly wind which blows periodically through mountain gaps of eastern Mexico. Violent 'Tehuantepecer events' have been observed to exceed 200 km/h. These winds drive strong coastal upwelling. Constrained by the gap in the mountains, the upwelling region is only ~50 km wide, and rapidly adjusts to form an oceanic eddy which then propagates slowly westward. It is known that the velocity structure of surface eddies in this region can penetrate to abyssal depths [*Demidova et al., 1993; Kontar and Sokov, 1994*] so a passing surface eddy can modify current speed and direction on the abyssal seafloor beneath.

Beginning in June 2012 a train of events began, clearly visible in satellite sea surface height fields (Figure 16a). Two eddies, one originating from eastern Mexico and the other from further south, most likely formed by the Papagayo gap-winds of Nicaragua, merged to form a single 'super-eddy'. Normally, Tehuantepecer eddies track westward at a latitude of approximately 12-13^0 north, but this 'super-eddy' propagated westward at around 15 to 20 cm/s at a lower latitude (Figure 16). This path led it directly over the mining areas of the CCZ some 318 days later and 4000 km from shore. This sequence of eddy genesis, merger and westward propagation is well captured in satellite sea surface height fields, from which surface geostrophic velocities may be calculated (Figure 16c). The unusual nature of the event is also evident in the satellite derived time series of eddy kinetic energy for the CCZ region (Figure 16b).

On April 11th 2013, just as the eddy was passing through the German CCZ area, BGR deployed three near-bed Doppler current meters (velocities shown in Figure 11, locations in Figure 1). Surface and near-bed velocities at all three sites show the influence of the eddy. Surface velocities peaked at 40 cm/s, and near bed velocities at 10 cm/s, lagged in time by 10 days or more. Though no sediment resuspension was observed, the intensity of these near-bed currents was unusual in long term records from this site.

To study the influence of such an eddy on a near-bed plume, the CCZ model was forced with a combination of observed currents, taken to be spatially uniform around the model boundary, and predicted tidal currents. The effect of the passing eddy can clearly be seen in the simulation (Figure 17). As the eddy passes, the direction of plume spreading backs to the north, elongating in that direction and dispersing the plume more rapidly. Eddy-induced increases in bed velocities have been reported to lead to significant resuspension and transport of bed material [*Zhang et al., 2014*], and this should also occur for previously settled tailings.

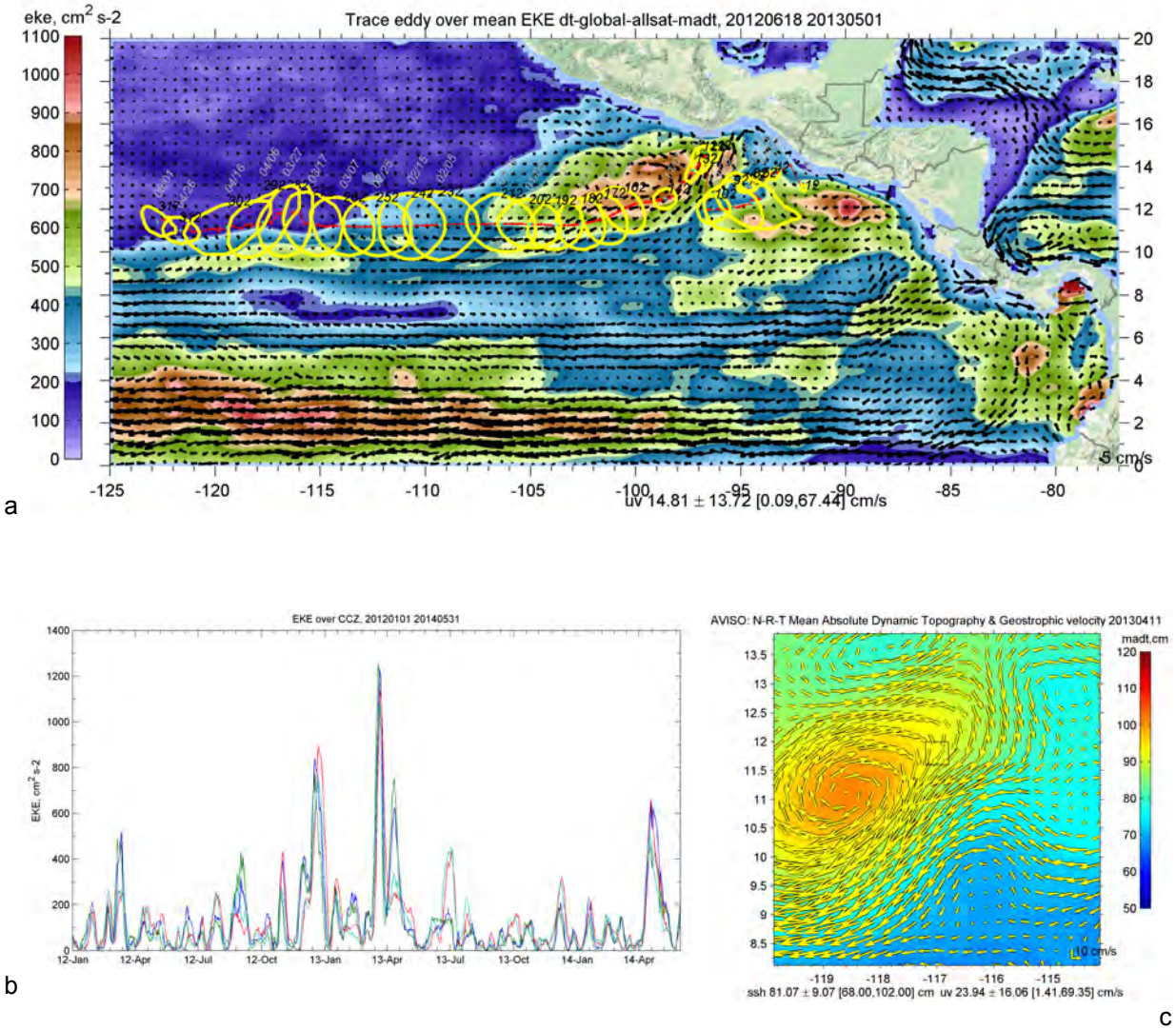

Figure 16: (a) Eddy track over 318 days since 2012/06/18 shown with yellow circles to indicate > 80 cm sea surface height (SSH) anomaly (MADT, AVISO) with 10-days intervals. Mean eddy kinetic energy (EKE) is shown with colours and superimposed with mean velocity vectors over period 2012-2014. (b)Timeseries of EKE over the mooring location, black arrow indicate the eddy propagation over the CCZ mooring site. (c) Surface geostrophic currents and Absolute Dynamic Topography in the area around the site (shown with rectangle [] *on the day of moorings deployment 2013/04/11.*

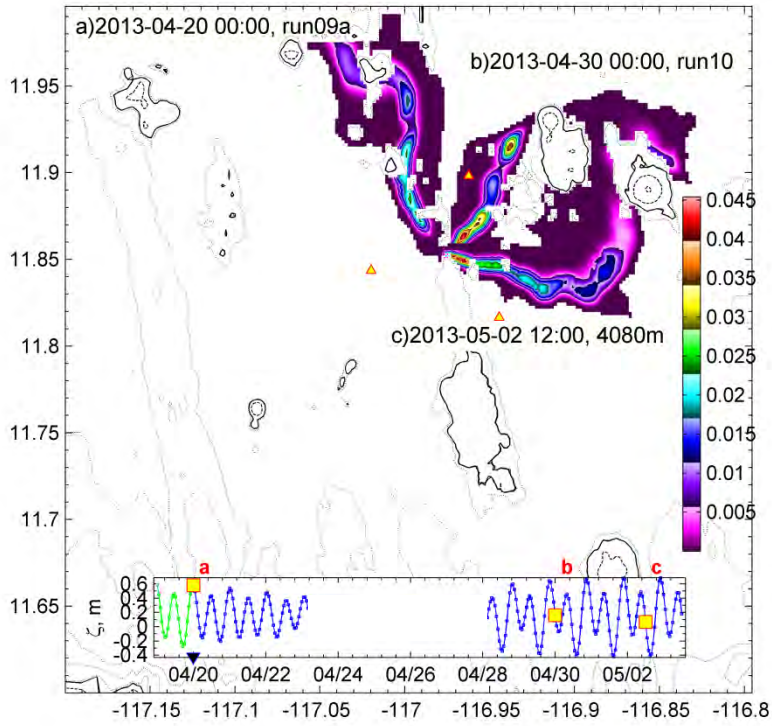

Figure 17: Colour shows modelled plume distribution in near seabed layers on three dates (a,b,c) in spring 2013 during and after large mesoscale eddy propagation over the area, which was detected with sea surface height anomaly using MADT (AVISO). Three RDI-ADCP 600kHz instruments were deployed 11th April 2013 at depth ~ 4128 m, 8 km apart near 11 0 52'N 116 0 58'W at BGR area of CCZ are shown with triangles Δ. Plume model has a 'permanent' constant source from the centre of mooring triangle.

5. Conclusions and further developments

Key results

High spatial resolution numerical model simulations, and the associated data analyses undertaken to confine the simulations to realistic scenarios, have revealed a number of key factors concerning sites typical of SMS deposits and polymetallic nodules:

For SMS deposit site on the MAR:

- Model simulations and the observed spread of a natural hydrothermal plume show excellent agreement.
- Local topography within a few hundred metres of the disturbance release strongly affects the initial plume spreading.
- Tidal flows are locally intensified by topographic constrictions.
- Internal tides of planar and spiral type are readily generated by the complex mix of ridges and spurs.
- Vertically propagating tidally generated internal waves carry tidal energy away from complex topographic slopes to remote and shallower parts of the water column in a complex and three dimensional manner.
- The direction of realistic mean flows superimposed on the model boundaries drastically effects the direction of plume spreading, but not the spreading rate.

For a typical polymetallic nodule site in the CCZ:

- Even at 4000 m depth, wind induced 'near-inertial' (NI) currents are as energetic as tidal currents.
- On time scales of hours to days, currents are dominated by tides and wind induced 'near-inertial' in equal measure.
- Near-inertial currents are not straightforward to model locally given their remote origin see below).
- On longer time scales, full depth ocean eddies dominate the near-bed currents, occasionally exceeding 10 cms^{-1}.
- The direction of realistic mean flows superimposed on the model boundaries drastically effects the direction of plume spreading, but less so the spreading rate.
- The passage of full depth ocean eddies changes the direction of plume spreading dramatically over a period one to several days.
- Topographic 'bumps' of the order of 100 m high by a few km wide have a number of profound effects on near bed flows:
    - Enhanced vertical mixing downstream is common as a result of internal hydraulics.
    - Downstream of a 'bump' mixing levels are sufficient to disperse material through a 100m thick bottom layer with a day
    - Large spatial variations in bottom currents are predicted: varying on the same spatial scale as topographic variations
    - Vertically propagating internal waves carry tidal and mean flow energy away from 'bumps' to remote and shallower parts of the water column in a non-trivial way

Model limitations: Remote effects

Flow structures in the ocean span a continuum of scales. Clearly, for a high resolution model with open boundaries to the surrounding ocean, there is no way to provide information on the full range of scales at the boundaries, even when the model is nested within a larger-scale model domain. Much

small scale complexity is locally-generated, however, extracting energy from large scale flows and tides. This component is included in a model of the sort described here. There will be an energy deficit, however, reflecting incoming energy from remote sources that are not represented in the local model. Perhaps the most notable omission is of propagating internal waves, including the general oceanic background internal wave field [*Garrett and Munk, 1975*], as well as the larger energy concentrations of the near-inertial frequency band and of the internal tide. The direct influence of near-inertial waves on a plume could be substantial, both distorting the plume and leading to enhanced shear and resulting mixing/diffusion.

Further model developments during MIDAS

To date, the modelling studies of WP2 have focussed on creating and verifying realistic simulations of neutrally buoyant discharges in domains typical of SMS deposits and polymetallic nodules. Further simulations and diagnostics are underway, specifically:

- Point release diffusion estimates. Rather than a continuous source of simulated discharge a number of simulations for both sites will be performed. The reason for this is somewhat technical, but in essence it allows for better determination of plume diffusion coefficient estimates than can be made with a continuous discharge
- Settling experiments. Using model velocity output from simulations already undertaken, a number of settling experiments will be undertaken. These will create maps of accumulation rate and total accumulation of a range of simulated particle sizes (with size represented by varying fall speeds)
- Comparisons between empirical parameter space ‘maps’ and model diagnostics. These comparisons are a vital step towards the final deliverable.
- A different model of the SMS deposit region has been run by MIDAS partners (IMAR). If time allows we will make a direct comparison between the MITgcm and MOHID model simulations of a SMS region of the MAR.

6. References

Dale, A. C., and M. E. Inall (2015), Tidal mixing processes amid small-scale, deep-ocean topography, Geophysical Research Letters, 42.

Demidova, T. A., E. A. Kontar, A. V. Sokov, and A. M. Belyaev (1993), The bottom currents in the area of abyssal hills in the north-east tropical Pacific Ocean, Phys. Oceanogr., 4(1), 53-61.

Dunphy, M. (2009), The influence of mesoscale eddies on the internal tide, 107 pp, University of Waterloo.

Egbert, G. D., and S. Y. Erofeeva (2002), Efficient Inverse Modeling of Barotropic Ocean Tides, Journal of Atmospheric and Oceanic Technology, 19(2), 183-204.

Garrett, C., and W. Munk (1975), Space-time scales of internal waves: A progress report, Journal of Geophysical Research, 80(3), 291-297.

Haney, R. L. (1991), On the Pressure Gradient Force over Steep Topography in Sigma Coordinate Ocean Models, Journal of Physical Oceanography, 21(4), 610-619, doi:10.1175/1520-0485(1991)021<0610:OTPGFO>2.0.CO;2.

Jackett, D. R., and T. J. Mcdougall (1995), Minimal adjustment of hydrographic profiles to achieve static stability, Journal of Atmospheric and Oceanic Technology, 12(2), 381-389.

Kontar, E. A., and A. V. Sokov (1994), A benthic storm in the northeastern tropical Pacific over the fields of manganese nodules, Deep Sea Research Part I: Oceanographic Research Papers, 41(7), 1069-1089.

Marshall, J., A. Adcroft, C. Hill, L. Perelman, and C. Heisey (1997), A finite-volume, incompressible Navier Stokes model for studies of the ocean on parallel computers, Journal of Geophysical Research: Oceans, 102(C3), 5753-5766, doi:10.1029/96JC02775.

Pacanowski, R. C., and S. G. H. Philander (1981), Parameterisation of Vertical Mixing in Numerical Models of Tropical Oceans, Journal of Physical Oceanography, 11, 1443 - 1451.

Roe, P. L. (1985), Some contributions to the modelling of discontinuous flows, paper presented at Large-scale computations in fluid mechanics; Proceedings of the Fifteenth Summer Seminar on Applied Mathematics, American Mathematical Society, La Jolla, CA, June 27-July 8, 1983.

Rühlemann, C., et al. (2014), MANGAN 2013 cruise report: Geology and biodiversity of the German License Area for the exploration of polymetallic nodules in the Equatorial NE PacificRep., 354 pp, Bundesanstalt für Geowissenschaften und Rohstoffe, Hannover.

Stashchuk, N., V. Vlasenko, M. E. Inall, and D. Aleynik (2014), Horizontal dispersion in shelf seas: High resolution modelling as an aid to sparse sampling, Progress in Oceanography, 128(0), 74-87, doi:http://dx.doi.org/10.1016/j.pocean.2014.08.007.

Thurnherr, A. M. (2006), Diapycnal mixing associated with an overflow in a deep submarine canyon, Deep Sea Research, Part II, 53(1-2), 194-206, doi:DOI:10.1016/j.dsr2.2005.10.020.

Thurnherr, A. M., K. J. Richards, C. R. German, G. F. Lane-Serff, and K. G. Speer (2002), Flow and mixing in the rift valley of the Mid-Atlantic Ridge, Journal of Physical Oceanography, 32(6), 1763-1778.

Wiedicke-Hombach, and e. al. (2009), Cruise report "Mangan 2008", RV Kilo Moana, 13 Oct. - 22 Nov. 2008Rep., 175 pp, Bundesanstalt fur Geowissenschaften und Rohstoffe, Hannover,.

Zhang, Y., Z. Liu, Y. Zhao, W. Wang, J. Li, and J. Xu (2014), Mesoscale eddies transport deep-sea sediments, Sci. Rep., 4.